



## 2013–2019 increases of surface ozone pollution in China: anthropogenic and meteorological influences

Ke Li<sup>1</sup>, Daniel J. Jacob<sup>1</sup>, Lu Shen<sup>1</sup>, Xiao Lu<sup>1</sup>, Isabelle De Smedt<sup>2</sup>, and Hong Liao<sup>3,4</sup>

<sup>1</sup>John A. Paulson School of Engineering and Applied Sciences, Harvard University, Cambridge, MA, USA

5 <sup>2</sup>Belgian Institute for Space Aeronomy (BIRA-IASB), Brussels, Belgium

<sup>3</sup>Jiangsu Key Laboratory of Atmospheric Environment Monitoring and Pollution Control, Collaborative Innovation Center of Atmospheric Environment and Equipment Technology, School of Environmental Science and Engineering, Nanjing University of Information Science and Technology, Nanjing, China

10 <sup>4</sup>Harvard-NUIST Joint Laboratory for Air Quality and Climate, Nanjing University of Information Science and Technology, Nanjing, China

*Correspondence to:* Ke Li (keli@seas.harvard.edu)

**Abstract.** Surface ozone data from the Chinese Ministry of Ecology and Environment (MEE) network show sustained increases across the country over the 2013–2019 period. Despite Phase 2 of Clean Air Action targeting ozone pollution, 15 ozone was higher in 2018–2019 than in previous years. The mean summer 2013–2019 trend of maximum 8-h average (MDA8) ozone was 1.9 ppb a<sup>-1</sup> across China and 3.3 ppb a<sup>-1</sup> in the North China Plain (NCP). Fitting ozone to meteorological variables with a multiple linear regression model shows that meteorology played a significant but not dominant role in the 2013–2019 ozone trend, contributing 0.70 ppb a<sup>-1</sup> across China and 1.4 ppb a<sup>-1</sup> in the NCP. Higher 20 June–July temperatures over the NCP were the main meteorological driver, particularly in recent years (2017–2019), and were associated with increased foehn winds. NCP data for 2017–2019 show a 15% continuing decrease in fine particulate matter (PM<sub>2.5</sub>) and flat emissions of volatile organic compounds (VOCs), which would explain the continued anthropogenic increase in ozone. VOC emission controls, as targeted by Phase 2 of the Chinese Clean Air Action, are needed to reverse the increase of ozone.



## 1 Introduction

Surface ozone is a serious air pollution issue over much of eastern China (Ma et al., 2012; Fu et al., 2019). Measurements from the Chinese Ministry of Environment and Ecology (MEE) network of sites frequently exceed the national air quality standard of  $160 \mu\text{g m}^{-3}$ , corresponding to 82 ppb at 298 K and 1013 hPa (Li et al., 2017; Shen et al., 2019a; Fan et al., 2020). The Clean Air Action initiated in 2013 imposed rapid decreases in pollutant emissions (Chinese State Council, 2013) and resulted in large decreases in fine particulate matter ( $\text{PM}_{2.5}$ ) concentrations (Zhai et al., 2019; Q. Zhang et al., 2019). However, ozone increased by 1–3 ppb  $\text{a}^{-1}$  over the 2013–2017 period in megacity clusters of eastern China (Lu et al., 2018; Li et al., 2019a; Lu et al. 2020), partly offsetting the health benefits from improved  $\text{PM}_{2.5}$  (Dang and Liao, 2019; Q. Zhang et al., 2019). Phase 2 of Clean Air Action starting in 2018 (Chinese State Council, 2018) imposed new emission controls targeted at ozone. Here we show that the increasing ozone trend in eastern China has continued through 2019, driven by both anthropogenic emission and meteorological trends, and stressing the urgent need for more vigorous emission controls.

Ozone in polluted regions is produced by photochemical reactions of volatile organic compounds (VOCs) and nitrogen oxides ( $\text{NO}_x \equiv \text{NO} + \text{NO}_2$ ), enabled by hydrogen oxide radicals ( $\text{HO}_x \equiv \text{OH} + \text{peroxy radicals}$ ) as oxidants. VOCs and  $\text{NO}_x$  are emitted by fuel combustion, and VOCs have additional industrial sources (Zheng et al., 2018).  $\text{HO}_x$  is produced photochemically from ozone and water, formaldehyde (HCHO), nitrous acid, and other precursors (Tan et al., 2019). Ozone is highest in summer when photochemistry is most active (Wang et al., 2017). Meteorological conditions play an important role in modulating ozone concentrations, not only through transport but also by affecting emissions and chemical rates (Jacob and Winner, 2009; Shen et al., 2016; Fu et al., 2019; Lu et al., 2019).

A number of studies have investigated the roles of anthropogenic and meteorological factors in driving the 2013–2017 ozone trend, and concluded that meteorological factors were not negligible but anthropogenic factors were dominant (Ding et al., 2019; Li et al., 2019a; Liu et al., 2019; Yu et al., 2019; Liu et al., 2020). Our previous work (Li et al., 2019a, 2019b) found that the decrease of  $\text{PM}_{2.5}$  was a major factor driving the increase of ozone due to the role of  $\text{PM}_{2.5}$  as scavenger of hydroperoxy ( $\text{HO}_2$ ) radicals and  $\text{NO}_x$  that would otherwise produce ozone. Here we extend the analysis of ozone trends to 2019, into the implementation of Clean Air Action Phase 2, and bring in satellite observations to relate the most recent ozone trends to those of VOC and  $\text{NO}_x$  emissions.

## 2 Data and methods

Hourly concentrations of ozone,  $\text{PM}_{2.5}$ , and  $\text{NO}_2$  are taken from the MEE website. The network was launched in 2013 as part of the Clean Air Action. It included 450 monitoring stations in 2013, growing to ~1500 stations by 2019. We



compute maximum daily 8-h average (MDA8) ozone and 24-h average PM<sub>2.5</sub> concentrations from the hourly data for June-August (JJA). Concentrations were reported by the MEE in units of  $\mu\text{g m}^{-3}$  under standard conditions (273 K, 1013 hPa) until 31 August 2018. This reference state was changed on 1 September 2018 to (298 K, 1013 hPa) for gases and local ambient state for PM<sub>2.5</sub> (MEE, 2018). We converted ozone concentrations to ppb, and rescaled post-August 2018 PM<sub>2.5</sub> concentrations to standard conditions by assuming (298 K, 1013 hPa) as the local ambient state.

We use observations of NO<sub>2</sub> and formaldehyde (HCHO) columns from the OMI and TROPOMI satellite instruments to track recent changes in anthropogenic emissions of NO<sub>x</sub> and VOCs, respectively. Shen et al. (2019b) and Shah et al. (2020) previously found that OMI-derived trends of VOC and NO<sub>x</sub> emissions were consistent with 2013–2017 bottom-up estimates from the Multi-resolution Emission Inventory for China (MEIC; Zheng et al., 2018). Here we extend the analysis using 2013–2019 OMI data from the European Quality Assurance for Essential Climate Variables project for NO<sub>2</sub> (Boersma et al., 2018) and HCHO (De Smedt et al., 2015). We further use TROPOMI data available for the summers of 2018–2019 for NO<sub>2</sub> (van Geffen et al., 2018) and HCHO (De Smedt et al., 2018). The TROPOMI data are freely accessed from <https://s5phub.copernicus.eu/dhus/> (last access: 28 February 2020) and we only use observations with quality assurance value larger than 0.75 for NO<sub>2</sub> and larger than 0.5 for HCHO. These filters effectively remove data with cloud fraction larger than 0.5. Interannual trends in HCHO columns could be affected by temperature-dependent emissions of biogenic VOCs (Palmer et al., 2006). Following Zhu et al. (2017), we remove this contribution by regressing June-July-August (JJA) monthly mean HCHO columns onto noon (13:00 local time) surface air temperatures, and then subtracting this fitted temperature dependency.

To quantify the role of meteorology in driving 2013–2019 ozone trends, we use the same stepwise multiple linear regression (MLR) modeling approach as Li et al. (2019a). This modeling approach relates the month-to-month variability of MDA8 ozone to that of meteorological variables. Consistent meteorological fields for 2013–2019 were obtained from the NASA Modern-Era Retrospective Analysis for Research and Applications, Version 2 (MERRA-2) product (<https://gmao.gsfc.nasa.gov/reanalysis/MERRA-2>, last access: 28 February 2020) (Gelaro et al., 2017). The MERRA-2 data have a spatial resolution of  $0.5^\circ$  latitude  $\times$   $0.625^\circ$  longitude. We average the daily MDA8 ozone from the MEE network onto the MERRA-2 grid. The regression model is first applied to select the key meteorological parameters driving the day-to-day variability of ozone for each grid cell. To avoid overfitting, only the three locally dominant meteorological parameters are regressed onto the deseasonalized monthly MDA8 ozone to fit the role of 2013–2019 meteorological variability. The trend in regressed ozone is taken to reflect the meteorological contribution, and the residual is then taken to reflect the anthropogenic contribution (Li et al., 2019a; Zhai et al., 2019).



### 3 Results and discussion

#### 3.1 2013–2019 ozone trends: anthropogenic and meteorological contributions

**Figure 1** shows 2013–2019 trends of summer maximum MDA8 ozone, summer mean MDA8 ozone, and summer mean  $PM_{2.5}$  from the MEE network. The Clean Air Action has dramatically improved  $PM_{2.5}$  pollution since 2013, with ~50% decrease of summertime  $PM_{2.5}$  concentrations across eastern China over the 2013–2019 period. In contrast, ozone has been steadily increasing over 2013–2019 and concentrations in 2019 are the highest in the record. The Clean Air Action focused specific attention on the four megacity clusters identified by rectangles. Mean MDA8 ozone in summer 2019 averaged 83 ppb across the North China Plain (NCP) and maximum MDA8 ozone averaged 129 ppb. Summer mean MDA8 ozone in 2019 was lower for the other megacity clusters (67 ppb for Yangtze River Delta (YRD), 46 ppb for Pearl River Delta (PRD), and 57 ppb for Sichuan Basin (SCB)) but summer maximum MDA8 ozone values were comparable to the NCP.

**Figure 2** (left panel) shows the 2013–2019 trends in summer mean MDA8 ozone obtained by ordinary linear regression of the data averaged over the  $0.5^\circ \times 0.625^\circ$  MERRA-2 grid. Ozone increases almost everywhere in China. Decreases are largely restricted to the Shandong Peninsula and Northeast China. The mean trend for China is  $1.9 \text{ ppb a}^{-1}$ . Trends in the four megacity clusters are  $3.3 \text{ ppb a}^{-1}$  for NCP,  $1.6 \text{ ppb a}^{-1}$  for YRD,  $1.1 \text{ ppb a}^{-1}$  for PRD, and  $0.7 \text{ ppb a}^{-1}$  for SCB (Table S1). The increases are largest in the NCP, where the effects of radical scavenging by  $PM_{2.5}$  would be largest (Li et al., 2019a, 2019b).

**Figure 2** (middle panel) shows the meteorologically driven ozone trends, as determined by fitting ozone to meteorological variables with the MLR model. We find an average meteorologically driven trend of  $0.7 \text{ ppb a}^{-1}$  for China. Ozone trends over 2013–2019 in the NCP and PRD are significantly enhanced by meteorology, and this is particularly driven by 2018–2019 (Table S1). Similar to our previous study for 2013–2017 (Li et al., 2019a), the most important meteorological predictor variables in the MLR model are daily maximum temperature for the NCP and meridional wind at 850 hPa for the PRD. These dominant meteorological parameters are also consistent with the findings from other studies (Gong and Liao, 2019; Wang et al., 2019; Han et al., 2020). Hot weather is the main meteorological driver for the NCP, and we will elaborate on this in the next section. The meteorological driver for ozone increase in the PRD is the weakened summer monsoonal southwesterlies (i.e., increased northeasterlies, Figure S1) that ventilate the PRD with marine air.

On the other hand, we find that meteorology mitigated ozone pollution increases over western China, northeastern China, and the Shandong Peninsula. Summer ozone in the Shandong Peninsula is strongly affected by maritime inflow (J. Zhang et al., 2019; Han et al., 2020) which increased over the 2013–2019 period (Figure S1).



Removing the meteorological contribution in the ozone trend leaves a residual trend that we interpret as anthropogenic (**Figure 2**, right panel). This anthropogenic trend is more uniformly positive than the observed and meteorologically driven trends. It averages  $1.2 \text{ ppb a}^{-1}$  for all of China, as compared to  $0.7 \text{ ppb a}^{-1}$  for the meteorologically driven trend. The observed 2013–2019 ozone increase in all the megacity clusters except the PRD is dominated by the anthropogenic contribution, averaging  $1.9 \text{ ppb a}^{-1}$  over the NCP. The following sections present further analysis of the ozone trends in the NCP, where both meteorological and anthropogenic contributions are particularly large.

### 3.2 Meteorologically driven 2013–2019 ozone increase in the North China Plain

Separating the observed 2013–2019 ozone trends by month (**Figure 3**) shows that the seasonal JJA trend of  $3.3 \text{ ppb a}^{-1}$  over the NCP is driven by June and July. Observed trends are  $5.5 \text{ ppb a}^{-1}$  for June,  $3.7 \text{ ppb a}^{-1}$  for July, and  $0.9 \text{ ppb a}^{-1}$  (statistically insignificant) for August. This month-to-month difference is mainly driven by meteorology. As derived from the MLR model, the meteorologically driven ozone trend of  $1.4 \text{ ppb a}^{-1}$  for JJA breaks down to  $3.1 \text{ ppb a}^{-1}$  for June,  $2.2 \text{ ppb a}^{-1}$  for July, and  $-1.0 \text{ ppb a}^{-1}$  (statistically insignificant) for August. The residual anthropogenic trend is much more similar across months ( $2.4 \text{ ppb a}^{-1}$  in June,  $1.5 \text{ ppb a}^{-1}$  in July,  $1.9 \text{ ppb a}^{-1}$  in August), as would be expected.

**Figure 3** shows the monthly mean time series of daily maximum temperature averaged over the NCP for 1980–2019, with 2013–2019 highlighted in shading. Temperature is the principal driver of the meteorologically driven ozone trend as indicated by the MLR model. We find a large 2013–2019 increase in temperature in June, a lesser increase in July, and a decrease in August, reflected in the meteorologically driven ozone trend for each month. When placed in the context of the 1980–2019 record, we see that the 2013–2019 temperature trends reflect interannual climate variability rather than a long-term warming trend.

Hot weather in the NCP in the summer is generally driven by large-scale anticyclonic conditions, and this has been viewed as the principal predictor of ozone pollution days (Gong and Liao, 2019). But foehn winds (Chen and Lu, 2016) are also important in June and to a lesser extent in July. Foehn winds blow from the mountains to the north and west, bringing warm and dry air to the NCP. By categorizing the 2013–2019 June circulation patterns between foehn-favorable and no-foehn conditions on the basis of the V850 foehn index (Chen and Lu, 2016), we find that foehn-favorable conditions are to a large extent responsible for the 2013–2019 increase in temperature in June (**Figure 4**). The frequency of foehn conditions under hot days in June increased by 85% over the 2013–2019 period, highlighting the previously unrecognized effect of foehn winds on ozone pollution in the NCP.



### 3.3 Anthropogenically driven 2013–2019 ozone increase in the North China Plain

**Figure 5a** shows the observed time series of monthly mean JJA MDA8 ozone anomalies in 2013–2019 relative to the JJA 2013–2019 mean, averaged over all MEE sites in the NCP. We see large month-to-month variability superimposed on the long-term trend. Much of this month-to-month variability can be attributed to meteorological factors using the  
5 MLR model (blue line), as discussed in the previous section. The residual anthropogenic trend (red line) shows a 2013–2019 increasing trend with much less month-to-month variability than the original observed time series.

**Figure 5b** shows the 2013–2019 observed trends of different quantities relevant to the anthropogenic ozone trend over the NCP:  $\text{PM}_{2.5}$  and  $\text{NO}_2$  from the MEE network, and  $\text{NO}_2$  and HCHO tropospheric columns from satellites.  $\text{PM}_{2.5}$  shows a steady decrease, 49% over the 2013–2019 period.  $\text{NO}_2$  (a proxy for  $\text{NO}_x$  emissions) shows a 25–30% decrease with  
10 some interannual variability that is consistent between the OMI satellite data and the surface MEE network. HCHO (a proxy of VOC emissions) shows no significant trend for the 2013–2019 period, with some interannual variability that could reflect noise in the measurement (Shen et al., 2019b).

Of particular interest are the trends for 2017–2019, extending beyond the currently available MEIC emission inventory (Zheng et al., 2018) and during which we find continued increase of ozone. We find for 2017–2019 a 15% decrease in  
15  $\text{PM}_{2.5}$ , a 6–10% decrease in  $\text{NO}_x$  emissions (depending on which proxy record we use), and flat VOC emissions. Phase 2 of the Chinese government's Clean Air Action (China State Council, 2018) called for a 18% decrease in  $\text{PM}_{2.5}$  over 2015–2020, a 15% decrease in  $\text{NO}_x$  emissions, and a 10% decrease in VOC emissions. Taking into account the already-achieved 2015–2017 gains in  $\text{PM}_{2.5}$  and  $\text{NO}_x$  emissions, Li et al. (2019b) inferred that those targets would require 2017–2020 decreases of 8% for  $\text{PM}_{2.5}$ , 9% for  $\text{NO}_x$  emissions, and 10% for VOCs emissions. They found from model  
20 simulations that the decrease in  $\text{PM}_{2.5}$  would cause further increase in ozone, but that decreasing VOC emissions would compensate and enable net improvement, with  $\text{NO}_x$  emission changes having relatively little effect. We find here that the observed 2017–2019 decrease in  $\text{PM}_{2.5}$  goes beyond the Clean Air Action target, while the satellite HCHO data show no evidence of a decrease in VOC emissions. Combination of these two effects is consistent with the observed anthropogenically driven increase in ozone over 2017–2019. Decrease of VOC emissions is the key to reverse the ozone  
25 increase (Li et al., 2019b).

## 4 Conclusions

Surface ozone data from the Chinese Ministry of Environment and Ecology (MEE) network show a sustained nationwide increase over the 2013–2019 period, with a few exceptions (Shandong Province, Northeast China), and with particularly high concentrations in 2018–2019. Correction for meteorological trends with a multiple linear regression (MLR) model



shows a general pattern of anthropogenically driven ozone increase across China, though meteorological influences are also significant. The mean summer (JJA) 2013–2019 increase in maximum daily 8-hour average (MDA8) ozone over China is 1.9 ppb a<sup>-1</sup>, including 0.7 ppb a<sup>-1</sup> from meteorological trends (mostly temperature and circulation) and 1.2 ppb a<sup>-1</sup> from anthropogenic influence. Ozone concentrations are highest in the North China Plain (NCP), where the summer mean MDA8 ozone averaged across sites was 83 ppb in 2019 and the summer maximum MDA8 ozone averaged across sites was 129 ppb. Mean summer MDA8 ozone increased by 3.3 ppb a<sup>-1</sup> in the NCP over the 2013–2019 period, which we attribute as 1.4 ppb a<sup>-1</sup> meteorological and 1.9 ppb a<sup>-1</sup> anthropogenic.

Further investigation of the NCP trends shows that hot weather in June–July 2018–2019 was a major driver for the high ozone concentrations in those summers. Such hot weather does not relate to long-term warming but to interannual variability driven principally by foehn northwesterly winds. Removing this meteorological variability shows a sustained anthropogenic ozone increase over the NCP persisting into 2018–2019. Examination of ozone-relevant anthropogenic variables from the MEE network and from satellites shows a 49% decrease in PM<sub>2.5</sub> for 2013–2019 (15% for 2017–2019), a 25–30% decrease in NO<sub>x</sub> emissions for 2013–2019 (6–10% for 2017–2019) and flat VOC emissions. The sustained anthropogenic increase in ozone over the 2017–2019 period can be explained by the continued decrease of PM<sub>2.5</sub>, which scavenges the radical precursors of ozone, combined with flat emissions of VOCs. Reducing VOC emissions should be the top priority for reversing the increase of ozone in the NCP and in other urban areas of China.

*Data availability.* The MERRA-2 reanalysis data are from <https://gmao.gsfc.nasa.gov/reanalysis/MERRA-2> (last access: 28 February 2020). The L3 OMI satellite data for NO<sub>2</sub> and HCHO are available at <http://www.qa4ecv.eu/ecvs> (last access: 28 February 2020). The L2 TROPOMI data for NO<sub>2</sub> and HCHO are freely available at <https://s5phub.copernicus.eu/dhus> (last access: 28 February 2020). The data used in this study can be accessed via doi (<https://doi.org/10.7910/DVN/T6D7YY>).

*Author contributions.* KL and DJJ designed the study. KL performed the analysis. LS and IDS provided the TROPOMI data. XL and HL contributed to the interpretation of the results. KL and DJJ wrote the paper with contributions from all co-authors

*Competing interests.* The authors declare that they have no conflict of interest.

*Acknowledgements.* This work is a contribution from the Harvard-NUIST Joint Laboratory for Air Quality and Climate. HL is supported by the National Natural Science Foundation of China (91744311). We appreciate the efforts from the China Ministry of Ecology and Environment for supporting the nationwide observation network and publishing hourly



air pollutant concentrations. We acknowledge the QA4ECV project for the NO<sub>2</sub> and HCHO data. We appreciate the efforts from NASA GMAO for providing the MERRA-2 reanalysis data.

## References

- Boersma, K. F., Eskes, H. J., Richter, A., De Smedt, I., Lorente, A., Beirle, S., van Geffen, J. H. G. M., Zara, M., Peters, E., Van Roozendaal, M., Wagner, T., Maasackers, J. D., van der A, R. J., Nightingale, J., De Rudder, A., Irie, H., Pinardi, G., Lambert, J.-C., and Compernelle, S. C.: Improving Algorithms and Uncertainty Estimates for Satellite NO<sub>2</sub> retrievals: Results from the Quality Assurance for the Essential Climate Variables (QA4ECV) Project, *Atmos. Meas. Tech.*, 11, 6651-6678, <http://dx.doi.org/10.5194/amt-11-6651-2018>, 2018.
- Chinese State Council: Action Plan on Air Pollution Prevention and Control (in Chinese), available at: [http://www.gov.cn/zwggk/2013-09/12/content\\_2486773.htm](http://www.gov.cn/zwggk/2013-09/12/content_2486773.htm) (last access: 28 February 2020), 2013.
- Chinese State Council: Three-Year Action Plan on Defending the Blue Sky (in Chinese), available at: [http://www.gov.cn/zhengce/content/2018-07/03/content\\_5303158.htm](http://www.gov.cn/zhengce/content/2018-07/03/content_5303158.htm) (last access: 28 February 2020), 2018
- Chen, R. and Lu, R.: Role of Large-Scale Circulation and Terrain in Causing Extreme Heat in Western North China, *J. Clim.*, 29, 2511-2527, <http://dx.doi.org/10.1175/jcli-d-15-0254.1>, 2016.
- Dang, R. and Liao, H.: Radiative Forcing and Health Impact of Aerosols and Ozone in China as the Consequence of Clean Air Actions over 2012–2017, *Geophys. Res. Lett.*, 46, 12511-12519, <https://doi.org/10.1029/2019GL084605>, 2019.
- De Smedt, I., Stavrou, T., Hendrick, F., Danckaert, T., Vlemmix, T., Pinardi, G., Theys, N., Lerot, C., Gielen, C., Vigouroux, C., Hermans, C., Fayt, C., Veefkind, P., Müller, J. F., and Van Roozendaal, M.: Diurnal, Seasonal and Long-Term Variations of Global Formaldehyde Columns Inferred from Combined Omi and Gome-2 Observations, *Atmos. Chem. Phys.*, 15, 12519-12545, <http://dx.doi.org/10.5194/acp-15-12519-2015>, 2015.
- De Smedt, I., Theys, N., Yu, H., Danckaert, T., Lerot, C., Compernelle, S., Van Roozendaal, M., Richter, A., Hilboll, A., Peters, E., Pedernana, M., Loyola, D., Beirle, S., Wagner, T., Eskes, H., van Geffen, J., Boersma, K. F., and Veefkind, P.: Algorithm Theoretical Baseline for Formaldehyde Retrievals from S5p Tropomi and from the QA4ECV Project, *Atmos. Meas. Tech.*, 11, 2395-2426, <http://dx.doi.org/10.5194/amt-11-2395-2018>, 2018.
- Ding, D., Xing, J., Wang, S., Chang, X., and Hao, J.: Impacts of Emissions and Meteorological Changes on China's Ozone Pollution in the Warm Seasons of 2013 and 2017, *Front. Environ. Sci. Eng.*, 13, 76, <http://dx.doi.org/10.1007/s11783-019-1160-1>, 2019.
- Fan, H., Zhao, C., and Yang, Y.: A Comprehensive Analysis of the Spatio-Temporal Variation of Urban Air Pollution in China During 2014–2018, *Atmos. Environ.*, 220, 117066, <http://dx.doi.org/10.1016/j.atmosenv.2019.117066>, 2020.





- Fu, Y., Liao, H., and Yang, Y.: Interannual and Decadal Changes in Tropospheric oOzone in China and the Associated Chemistry-Climate Interactions: A Review, *Adv. Atmos. Sci.*, 36, 975-993, <https://doi.org/10.1007/s00376-019-8216-9>, 2019
- 5 Gelaro, R., McCarty, W., Suarez, M. J., Todling, R., Molod, A., Takacs, L., Randles, C., Darmenov, A., Bosilovich, M. G., Reichle, R., Wargan, K., Coy, L., Cullather, R., Draper, C., Akella, S., Buchard, V., Conaty, A., da Silva, A., Gu, W., Kim, G. K., Koster, R., Lucchesi, R., Merkova, D., Nielsen, J. E., Partyka, G., Pawson, S., Putman, W., Rienecker, M., Schubert, S. D., Sienkiewicz, M., and Zhao, B.: The Modern-Era Retrospective Analysis for Research and Applications, Version 2 (MERRA-2), *J. Clim.*, 30, 5419-5454, <http://dx.doi.org/10.1175/JCLI-D-16-0758.1>, 2017.
- 10 Gong, C. and Liao, H.: A Typical Weather Pattern for Ozone Pollution Events in North China, *Atmos. Chem. Phys.*, 19, 13725-13740, <http://dx.doi.org/10.5194/acp-19-13725-2019>, 2019.
- Han, H., Liu, J., Shu, L., Wang, T., and Yuan, H.: Local and Synoptic Meteorological Influences on Daily Variability in Summertime Surface Ozone in Eastern China, *Atmos. Chem. Phys.*, 20, 203-222, <http://dx.doi.org/10.5194/acp-20-203-2020>, 2020.
- 15 Jacob, D. J. and Winner, D. A.: Effect of Climate Change on Air Quality, *Atmos. Environ.*, 43, 51-63, <http://dx.doi.org/10.1016/j.atmosenv.2008.09.051>, 2009.
- Li, G., Bei, N., Cao, J., Wu, J., Long, X., Feng, T., Dai, W., Liu, S., Zhang, Q., and Tie, X.: Widespread and Persistent Ozone Pollution in Eastern China During the Non-Winter Season of 2015: Observations and Source Attributions, *Atmos. Chem. Phys.*, 17, 2759-2774, <http://dx.doi.org/10.5194/acp-17-2759-2017>, 2017.
- 20 Li, K., Jacob, D. J., Liao, H., Shen, L., Zhang, Q., and Bates, K. H.: Anthropogenic Drivers of 2013-2017 Trends in Summer Surface Ozone in China, *Proc. Natl. Acad. Sci. U.S.A.*, 116, 422-427, <http://dx.doi.org/10.1073/pnas.1812168116>, 2019a.
- Li, K., Jacob, D. J., Liao, H., Zhu, J., Shah, V., Shen, L., Bates, K. H., Zhang, Q., and Zhai, S.: A Two-Pollutant Strategy for Improving Ozone and Particulate Air Quality in China, *Nat. Geosci.*, 12, 906-910, <http://dx.doi.org/10.1038/s41561-019-0464-x>, 2019b.
- 25 Liu, J., Wang, L., Li, M., Liao, Z., Sun, Y., Song, T., Gao, W., Wang, Y., Li, Y., Ji, D., Hu, B., Kerminen, V.-M., Wang, Y., and Kulmala, M.: Quantifying the Impact of Synoptic Circulation Patterns on Ozone Variability in Northern China from April to October 2013-2017, *Atmos. Chem. Phys.*, 19, 14477-14492, <http://dx.doi.org/10.5194/acp-19-14477-2019>, 2019.
- 30 Liu, Y. and Wang, T.: Worsening urban ozone pollution in China from 2013 to 2017 – Part 1: The complex and varying roles of meteorology, *Atmos. Chem. Phys. Discuss.*, <https://doi.org/10.5194/acp-2019-1120>, in review, 2020.



- Lorente, A., Boersma, K. F., Eskes, H. J., Veeffkind, J. P., van Geffen, J., de Zeeuw, M. B., Denier van der Gon, H. A. C., Beirle, S., and Krol, M. C.: Quantification of Nitrogen Oxides Emissions from Build-up of Pollution over Paris with Tropomi, *Sci. Rep.*, 9, 20033, <http://dx.doi.org/10.1038/s41598-019-56428-5>, 2019.
- Lu, X., Hong, J., Zhang, L., Cooper, O. R., Schultz, M. G., Xu, X., Wang, T., Gao, M., Zhao, Y., and Zhang, Y.: Severe Surface Ozone Pollution in China: A Global Perspective, *Environ. Sci. Technol. Lett.*, 5, 487-494, <http://dx.doi.org/10.1021/acs.estlett.8b00366>, 2018.
- Lu, X., Zhang, L., and Shen, L.: Meteorology and Climate Influences on Tropospheric Ozone: A Review of Natural Sources, Chemistry, and Transport Patterns, *Curr. Pollut. Rep.*, 5, 238-260, <http://dx.doi.org/10.1007/s40726-019-00118-3>, 2019.
- Lu, X., Zhang, L., Wang, X., Gao, M., Li, K., Zhang, Y., Yue, X., and Zhang, Y.: Rapid Increases in Warm-Season Surface Ozone and Resulting Health Impact in China since 2013, *Environ. Sci. Technol. Lett.*, <http://dx.doi.org/10.1021/acs.estlett.0c00171>, 2020.
- Ma, J., Xu, X., Zhao, C., and Yan, P.: A Review of Atmospheric Chemistry Research in China: Photochemical Smog, Haze Pollution, and Gas-Aerosol Interactions, *Adv. Atmos. Sci.*, 29, 1006-1026, <http://dx.doi.org/10.1007/s00376-012-1188-7>, 2012.
- Ministry of Ecology and Environment (MEE): Revision of the Ambient air quality standards (GB 3095-2012) (in Chinese), available at: [http://www.mee.gov.cn/xxgk/2018/xxgk/xxgk01/201808/t20180815\\_629602.html](http://www.mee.gov.cn/xxgk/2018/xxgk/xxgk01/201808/t20180815_629602.html) (last access: 28 February 2020), 2018.
- Palmer, P. I., Abbot, D. S., Fu, T.-M., Jacob, D. J., Chance, K., Kurosu, T. P., Guenther, A., Wiedinmyer, C., Stanton, J. C., Pilling, M. J., Pressley, S. N., Lamb, B., and Sumner, A. L.: Quantifying the Seasonal and Interannual Variability of North American Isoprene Emissions Using Satellite Observations of the Formaldehyde Column, *J. Geophys. Res.*, 111, <http://dx.doi.org/10.1029/2005jd006689>, 2006.
- Shah, V., Jacob, D. J., Li, K., Silvern, R. F., Zhai, S., Liu, M., Lin, J., and Zhang, Q.: Effect of Changing NO<sub>x</sub> Lifetime on the Seasonality and Long-Term Trends of Satellite-Observed Tropospheric NO<sub>2</sub> Columns over China, *Atmos. Chem. Phys.*, 20, 1483-1495, <http://dx.doi.org/10.5194/acp-20-1483-2020>, 2020.
- Shen, L., Mickley, L. J., and Gilleland, E.: Impact of increasing heat waves on US ozone episodes in the 2050s: Results from a multimodel analysis using extreme value theory, *Geophys. Res. Lett.*, 43, 4017-4025, <http://dx.doi.org/10.1002/2016GL068432>, 2016.
- Shen, L., Jacob, D. J., Liu, X., Huang, G., Li, K., Liao, H., and Wang, T.: An Evaluation of the Ability of the Ozone Monitoring Instrument (OMI) to Observe Boundary Layer Ozone Pollution across China: Application to 2005–2017 Ozone Trends, *Atmos. Chem. Phys.*, 19, 6551-6560, <http://dx.doi.org/10.5194/acp-19-6551-2019>, 2019a.



- Shen, L., Jacob, D. J., Zhu, L., Zhang, Q., Zheng, B., Sulprizio, M. P., Li, K., De Smedt, I., González Abad, G., Cao, H., Fu, T. M., and Liao, H.: The 2005–2016 Trends of Formaldehyde Columns over China Observed by Satellites: Increasing Anthropogenic Emissions of Volatile Organic Compounds and Decreasing Agricultural Fire Emissions, *Geophys. Res. Lett.*, 46, 4468–4475, <http://dx.doi.org/10.1029/2019gl082172>, 2019b.
- 5 Tan, Z., Lu, K., Jiang, M., Su, R., Wang, H., Lou, S., Fu, Q., Zhai, C., Tan, Q., Yue, D., Chen, D., Wang, Z., Xie, S., Zeng, L., and Zhang, Y.: Daytime Atmospheric Oxidation Capacity in Four Chinese Megacities During the Photochemically Polluted Season: A Case Study Based on Box Model Simulation, *Atmos. Chem. Phys.*, 19, 3493–3513, <http://dx.doi.org/10.5194/acp-19-3493-2019>, 2019.
- van Geffen, J. H. G. M., Eskes, H. J., Boersma, K. F., Maasakkers, J. D., and Veeffkind, J. P.: TROPOMI ATBD of the total and tropospheric NO<sub>2</sub> data products (issue 1.2.0), Royal Netherlands Meteorological Institute (KNMI), De Bilt, the Netherlands, s5P-KNMI-L2-0005-RP, 2018.
- 10 Wang, T., Xue, L., Brimblecombe, P., Lam, Y. F., Li, L., and Zhang, L.: Ozone Pollution in China: A Review of Concentrations, Meteorological Influences, Chemical Precursors, and Effects, *Sci. Total. Environ.*, 575, 1582–1596, <http://dx.doi.org/10.1016/j.scitotenv.2016.10.081>, 2017.
- 15 Wang, T., Dai, J., Lam, K. S., Nan Poon, C., and Brasseur, G. P.: Twenty-Five Years of Lower Tropospheric Ozone Observations in Tropical East Asia: The Influence of Emissions and Weather Patterns, *Geophys. Res. Lett.*, 46, 11463–11470, <https://doi.org/10.1029/2019GL084459>, 2019
- Yu, Y., Wang, Z., He, T., Meng, X., Xie, S., and Yu, H.: Driving Factors of the Significant Increase in Surface Ozone in the Yangtze River Delta, China, During 2013–2017, *Atmos. Pollut. Res.*, 10, 1357–1364, <http://dx.doi.org/10.1016/j.apr.2019.03.010>, 2019.
- 20 Zhai, S., Jacob, D. J., Wang, X., Shen, L., Li, K., Zhang, Y., Gui, K., Zhao, T., and Liao, H.: Fine Particulate Matter (PM<sub>2.5</sub>) Trends in China, 2013–2018: Separating Contributions from Anthropogenic Emissions and Meteorology, *Atmos. Chem. Phys.*, 19, 11031–11041, <http://dx.doi.org/10.5194/acp-19-11031-2019>, 2019.
- Zhang, J., Wang, C., Qu, K., Ding, J., Shang, Y., Liu, H., and Wei, M.: Characteristics of Ozone Pollution, Regional Distribution and Causes During 2014–2018 in Shandong Province, East China, *Atmosphere*, 10, <http://dx.doi.org/10.3390/atmos10090501>, 2019.
- 25 Zhang, Q., Zheng, Y., Tong, D., Shao, M., Wang, S., Zhang, Y., Xu, X., Wang, J., He, H., Liu, W., Ding, Y., Lei, Y., Li, J., Wang, Z., Zhang, X., Wang, Y., Cheng, J., Liu, Y., Shi, Q., Yan, L., Geng, G., Hong, C., Li, M., Liu, F., Zheng, B., Cao, J., Ding, A., Gao, J., Fu, Q., Huo, J., Liu, B., Liu, Z., Yang, F., He, K., and Hao, J.: Drivers of Improved PM<sub>2.5</sub> Air Quality in China from 2013 to 2017, *Proc. Natl. Acad. Sci. U.S.A.*, 116, 24463–24469, <http://dx.doi.org/10.1073/pnas.1907956116>, 2019.
- 30



Zheng, B., Tong, D., Li, M., Liu, F., Hong, C., Geng, G., Li, H., Li, X., Peng, L., Qi, J., Yan, L., Zhang, Y., Zhao, H., Zheng, Y., He, K., and Zhang, Q.: Trends in China's Anthropogenic Emissions since 2010 as the Consequence of Clean Air Actions, *Atmos. Chem. Phys.*, 18, 14095–14111, <http://dx.doi.org/10.5194/acp-18-14095-2018>, 2018.

Zhu, L., Mickley, L. J., Jacob, D. J., Marais, E. A., Sheng, J., Hu, L., González Abad, G., and Chance, K.: Long-term (2005–2014) trends in formaldehyde (HCHO) columns across North America as seen by the OMI satellite instrument: Evidence of changing emissions of volatile organic compounds. *Geophys. Res. Lett.*, 44, 7079–7086, <http://dx.doi.org/10.1002/2017GL073859>, 2017.

### Figure captions

10 **Figure 1.** Summer (JJA) maximum MDA8 ozone (top), summer mean MDA8 ozone (middle), and summer mean PM<sub>2.5</sub> (bottom) for 2013–2019 at the network operated by the China Ministry of Ecology and Environment (MEE). Rectangles denote the four megacity clusters discussed in the text: North China Plain (NCP; 34°–41°N, 113°–119°E), Yangtze River Delta (YRD, 30°–33°N, 119°–122°E), Pearl River Delta (PRD, 21.5°–24°N, 112°–115.5°E), and Sichuan Basin (SCB, 28.5°–31.5°N, 103.5°–107°E).

15 **Figure 2.** Summertime ozone trends in China, 2013–2019. The left panel (a) shows observed trends of summer mean MDA8 ozone at MEE sites averaged on the  $0.5^\circ \times 0.625^\circ$  ( $\approx 50 \times 50 \text{ km}^2$ ) MERRA-2 grid. The trends are obtained by ordinary linear regression and include sites with partial records. The middle panel (b) shows meteorologically driven trends determined by fitting ozone to meteorological covariates in the multiple linear regression (MLR) model. The right panel (c) shows anthropogenic trends as inferred from the residual of the MLR model. Statistically significant trends  
20 above the 90% confidence level are marked with black dots. The mean trends for all of China and for the four megacity clusters are inset, where the regression is applied to the spatially averaged MDA8 ozone for the cluster. Numbers in bold are statistically significant above the 90% confidence level.

**Figure 3.** Time series of June–August daily maximum surface air temperatures over the North China Plain (NCP) for 1980–2019. Values are monthly means from the MERRA-2 reanalysis. The 2013–2019 period for the ozone trend  
25 analysis is shaded in grey. The observed (OBS), meteorologically-driven (MET), and anthropogenically-driven (ANTH) monthly ozone trends ( $\text{ppb a}^{-1}$ ) in the NCP for 2013–2019 are shown in the table to the right, where numbers in bold are statistically significant above the 90% confidence level.

**Figure 4.** June mean trends in meteorological variables over 2013–2019 under foehn-favorable (top) and non-foehn conditions (bottom). (a) Trends in 850 hPa winds ( $\text{m s}^{-1} \text{ a}^{-1}$ ) and surface daily maximum temperature ( $^\circ\text{C a}^{-1}$ , shaded)  
30 under foehn-favorable conditions; (b) Trends in 500 hPa winds ( $\text{m s}^{-1} \text{ a}^{-1}$ ) and surface relative humidity ( $\% \text{ a}^{-1}$ , shaded)



under foehn-favorable conditions. **(c, d)** are the same as **(a, b)** but for non-foehn conditions. Data are from the MERRA-2 re-analysis and trends are obtained by ordinary linear regression. Foehn conditions are diagnosed a foehn index V850 defined by the 850 hPa northwesterly wind averaged along a section from (42°N, 108°E) to (38°N, 112°E) (green line in **a**). The days with positive (negative) V850 are taken as foehn-favorable (no-foehn) condition. The frequency of foehn wind under hot days increased by 85% over the period. Data are from the MERRA-2 reanalysis.

**Figure 5.** Trends in summertime ozone and related anthropogenic drivers in the North China Plain (NCP). The left panel **(a)** shows time series of monthly mean MDA8 ozone (ppb) anomalies averaged over the MEE sites relative to the 2013–2019 summer (JJA) mean. Values are shown as anomalies for individual JJA months (3 points per year). Observed trends are compared to the meteorologically driven trends diagnosed by the MLR model, and to the residuals determining the anthropogenically driven trend. The right panel **(b)** shows time series of observed JJA mean quantities averaged over the NCP: PM<sub>2.5</sub> and NO<sub>2</sub> concentrations from the MEE sites, and tropospheric NO<sub>2</sub> and HCHO column densities from the OMI and TROPOMI satellite instruments. Values are presented as ratios relative to 2013. The TROPOMI data for 2018 have been scaled to the OMI data for that year with the multiplicative factor indicated in legend. The low bias for TROPOMI NO<sub>2</sub> is similar with the finding by Lorente et al. (2019).

15

20

25

30

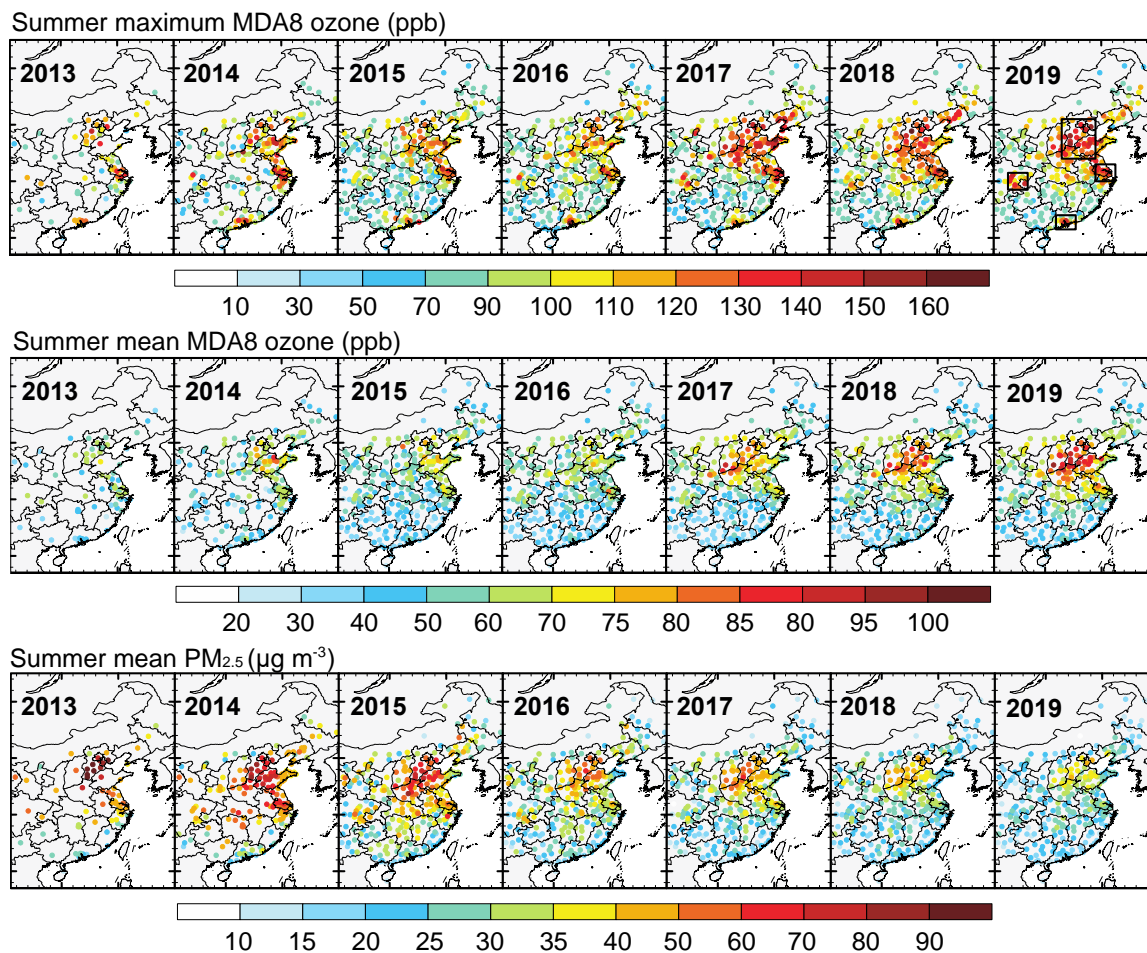


**Figure 1.** Summer (JJA) maximum MDA8 ozone (top), summer mean MDA8 ozone (middle), and summer mean PM<sub>2.5</sub> (bottom) for 2013–2019 at the network operated by the China Ministry of Ecology and Environment (MEE). Rectangles denote the four megacity clusters discussed in the text: North China Plain (NCP; 34°–41°N, 113°–119°E), Yangtze River Delta (YRD, 30°–33°N, 119°–122°E), Pearl River Delta (PRD, 21.5°–24°N, 112°–115.5°E), and Sichuan Basin (SCB, 28.5°–31.5°N, 103.5°–107°E).



### 2013-2019 summertime MDA8 ozone trends

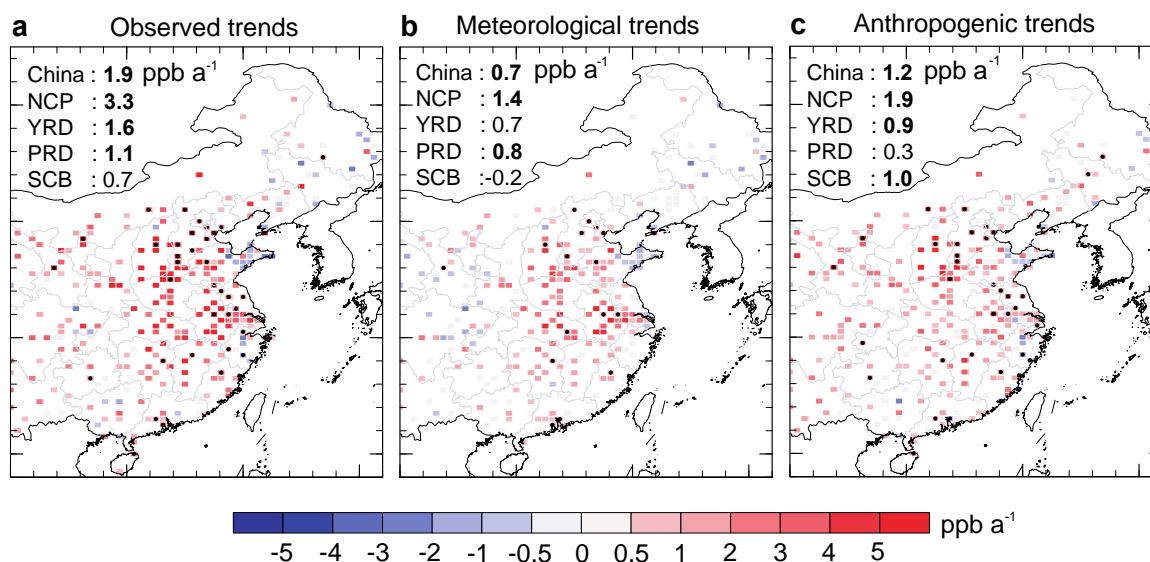


**Figure 2.** Summertime ozone trends in China, 2013–2019. The left panel (a) shows observed trends of summer mean MDA8 ozone at MEE sites averaged on the  $0.5^\circ \times 0.625^\circ$  ( $\approx 50 \times 50 \text{ km}^2$ ) MERRA-2 grid. The trends are obtained by ordinary linear regression and include sites with partial records. The middle panel (b) shows meteorologically driven trends determined by fitting ozone to meteorological covariates in the multiple linear regression (MLR) model. The right panel (c) shows anthropogenic trends as inferred from the residual of the MLR model. Statistically significant trends above the 90% confidence level are marked with black dots. The mean trends for all of China and for the four megacity clusters are inset, where the regression is applied to the spatially averaged MDA8 ozone for the cluster. Numbers in bold are statistically significant above the 90% confidence level.

15

20

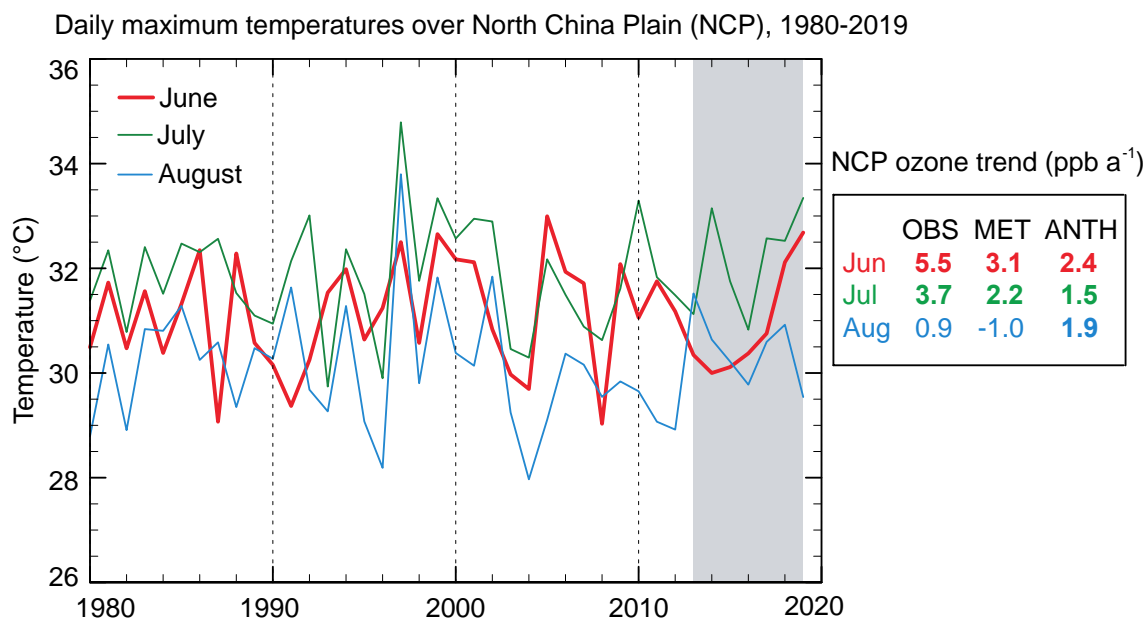


**Figure 3.** Time series of June-August daily maximum surface air temperatures over the North China Plain (NCP) for 1980–2019. Values are monthly means from the MERRA-2 reanalysis. The 2013–2019 period for the ozone trend analysis is shaded in grey. The observed (OBS), meteorologically-driven (MET), and anthropogenically-driven (ANTH) monthly ozone trends ( $\text{ppb a}^{-1}$ ) in the NCP for 2013–2019 are shown in the table to the right, where numbers in bold are statistically significant above the 90% confidence level.

10

15





June meteorology trends over 2013–2019 under foehn-favorable (top) and non-foehn (bottom) conditions

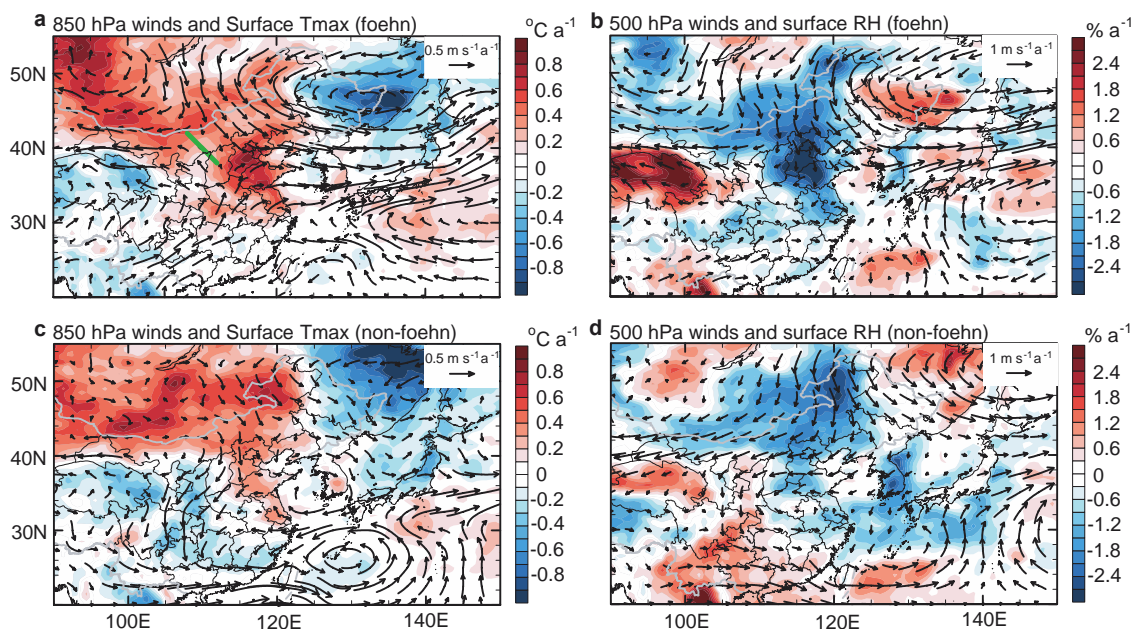


**Figure 4.** June mean trends in meteorological variables over 2013–2019 under foehn-favorable (top) and non-foehn conditions (bottom). **(a)** Trends in 850 hPa winds ( $\text{m s}^{-1} \text{a}^{-1}$ ) and surface daily maximum temperature ( $^{\circ}\text{C a}^{-1}$ , shaded) under foehn-favorable conditions; **(b)** Trends in 500 hPa winds ( $\text{m s}^{-1} \text{a}^{-1}$ ) and surface relative humidity ( $\% \text{a}^{-1}$ , shaded) under foehn-favorable conditions. **(c, d)** are the same as **(a, b)** but for non-foehn conditions. Data are from the MERRA-2 re-analysis and trends are obtained by ordinary linear regression. Foehn conditions are diagnosed a foehn index V850 defined by the 850 hPa northwesterly wind averaged along a section from ( $42^{\circ}\text{N}$ ,  $108^{\circ}\text{E}$ ) to ( $38^{\circ}\text{N}$ ,  $112^{\circ}\text{E}$ ) (green line in **a**). The days with positive (negative) V850 are taken as foehn-favorable (no-foehn) condition. The frequency of foehn wind under hot days increased by 85% over the period. Data are from the MERRA-2 reanalysis.



Trends in summertime ozone and anthropogenic drivers in the North China Plain

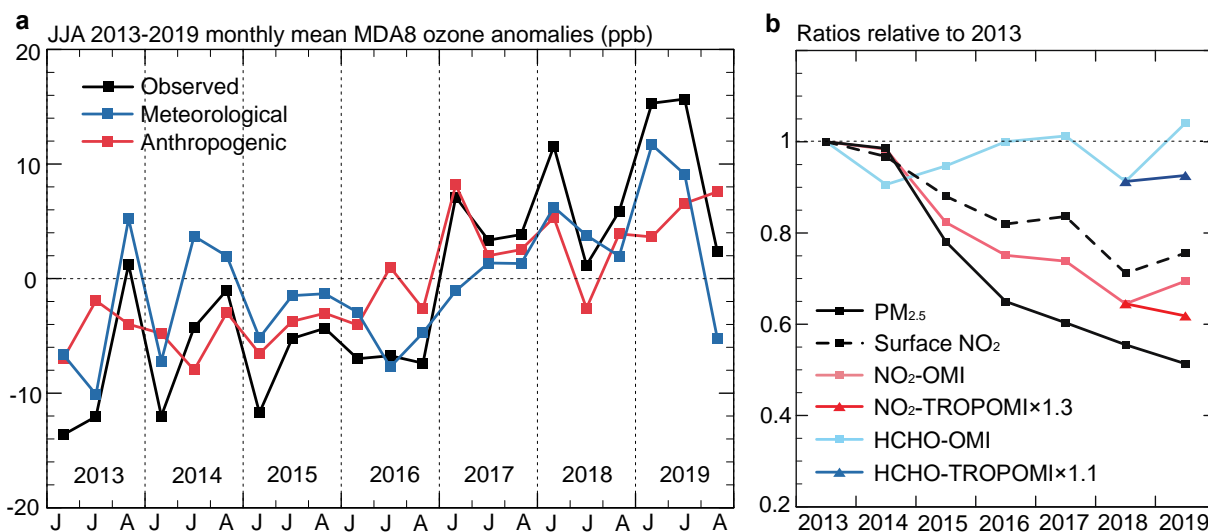


**Figure 5.** Trends in summertime ozone and related anthropogenic drivers in the North China Plain (NCP). The left panel (a) shows time series of monthly mean MDA8 ozone (ppb) anomalies averaged over the MEE sites relative to the 2013–2019 summer (JJA) mean. Values are shown as anomalies for individual JJA months (3 points per year). Observed trends are compared to the meteorologically driven trends diagnosed by the MLR model, and to the residuals determining the anthropogenically driven trend. The right panel (b) shows time series of observed JJA mean quantities averaged over the NCP: PM<sub>2.5</sub> and NO<sub>2</sub> concentrations from the MEE sites, and tropospheric NO<sub>2</sub> and HCHO column densities from the OMI and TROPOMI satellite instruments. Values are presented as ratios relative to 2013. The TROPOMI data for 2018 have been scaled to the OMI data for that year with the multiplicative factor indicated in legend. The low bias for TROPOMI NO<sub>2</sub> is similar with the finding by Lorente et al. (2019).